Theoretical and Applied Fracture Mechanics 137 (2025) 104869

Contents lists available at ScienceDirect

Theoretical and Applied Fracture Mechanics

journal homepage: www.elsevier.com/locate/tafmec

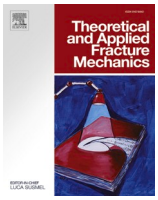

Reverse bend experiments on the base plate and discussion of the appropriate amount of reverse bending for precrack straightness (Effect of the reverse bend process on the CTOD toughness evaluation and understanding of its mechanisms)

Tomoya Kawabata [a,*], Hoichi Kitano [b], Takumi Ozawa [c], Yoshiki Mikami [d]

[a] Department of Systems Innovation, The University of Tokyo, Tokyo 113-8656, Japan
[b] National Institute for Materials Science, Tsukuba 305-0047, Japan
[c] National Maritime Research Institute, Mitaka 181-0004, Japan
[d] Joining & Welding Research Institute, Osaka University, Suita 567-0047, Japan

ARTICLE INFO

Keywords:
CTOD
Standard
Reverse bend
Weibull stress

ABSTRACT

Measurements of the critical value of the crack-tip opening displacement (CTOD) of welded joints often suffer from weld residual stresses, which prevent the introduction of a straight precrack front. In this study, the effects of reverse bending, a proven method for straightening the crack front shape, on evaluations of the critical CTOD are investigated. To compare the differences in the evaluation results, the authors used a base plate without residual stress inside the material for their experiments. Five different reverse bending treatments were applied to a 50 mm thick base metal, and the effects of reverse bending were evaluated via CTOD tests at low temperatures. Additionally, numerical simulations were carried out via the finite element method to exclude the effects of a_0/W and a_f, which cannot be unified in the experiments, and to understand the mechanism. After reverse bending and unloading, the tensile residual stress is distributed at the notch edge, and a high stress intensity at the fatigue crack tip during CTOD testing can be expected. In addition, when the amount of reverse bending is increased to $L_r = 1.35$, the compressive residual stress distribution in front of the specimen expands, and the P–V_g curve clearly decreases, which may impair the precrack shape flatness. Therefore, the controlled range of L_r should be at least less than 1.35.

1. Introduction

The prevention of brittle fracture incidents, which can cause catastrophic damage and loss of life, is a major concern for all equipment and machinery industries. Fracture mechanics research, which started in Europe and the United States after World War II, has become a significant trend in Japan in response to the rise of heavy industries. Fracture assessments, which use crack-tip opening displacement (CTOD) [1] as a fracture mechanics parameter, have been widely used in many fields, such as heavy industry and energy. The critical values are examined not only for base materials but also for welded joints. Evaluating the critical value of welded joints, which are more likely to contain defects and have a greater fracture risk, is essential. During an evaluation, introducing a fatigue precrack is necessary for analyzing unstable fractures from the crack edge. However, when assessing welded joints, the distribution of residual stresses due to the thermal stress during welding prevents the introduction of a precrack at the thickness position [2] (as exemplified in Fig. 1 [3]). Therefore, since the establishment of the CTOD test method, a pretreatment method has been investigated to solve this problem and ensure flat precracking throughout the thickness of the welded joint [2]. In ISO 15653 [4], the most widely used standard for evaluating the CTOD in welded joints, two pretreatment methods before the introduction of a precrack are listed in Annex C, namely, reverse bending and local compression. Via both methods, the residual stress distribution is changed by applying plastic deformation to a part, including the notch root, to straighten the crack propagation shape. This series of papers focuses on reverse bending, as illustrated in Fig. 2. According to The Welding Institute (TWI) [2], the first record of the reverse bending method was reported in 1976 in the United States [5], where it was used for stress corrosion cracking tests. In addition, significant research on the application of the reverse bending technique for

* Corresponding author.
E-mail address: kawabata@fract.t.u-tokyo.ac.jp (T. Kawabata).

https://doi.org/10.1016/j.tafmec.2025.104869
Received 23 October 2024; Received in revised form 12 January 2025; Accepted 6 February 2025
Available online 13 February 2025

Nomenclature

a_0	Initial crack length
a_{av}	Weight-averaged total crack length, that is, the sum of a_M and $a_{f,av}$
a_f	Fatigue crack length
$a_{f,av.}$	Average fatigue crack length
$a_{f,max}$	Maximum of nine measurements a_f along the fatigue crack front
$a_{f,min}$	Minimum of nine measurements a_f along the fatigue crack front
Δa_f	The crack length difference between $a_{f,max}$ and $a_{f,min}\{i = 2–8\}$
a_M	Machined notch length
B	Specimen thickness
d	Distance from notch tip
f	A function to evaluate whether the envelope specified in the CTOD test standard is satisfied.
k	a_f/ω_{RB}
$K_{\text{Point stress},x}$	Stress intensity factor by point stress used in the Dugdale model
$K_{\sum \text{Point stress}}$	Superposed stress intensity factor by point stress at position x used in the Dugdale model
K_{RB}	Stress intensity factor of the machined notch induced by the reverse bending load
$K_{\text{Remote stress}}$	Stress intensity factor by reverse bending force
$K_{\Delta\sigma_{eff}}$	K value change due to effective stress variation $\Delta\sigma_{eff}(\sigma_{unload}\text{-}\sigma_{comp})$
L_r	Load ratio of P_{RB} to P_L
M	Moment
m	Shape parameter of Weibull distribution of critical CTOD
N	Notch width
n	Work hardening exponent in the Swift relationship
P	Load, Force
P_L	Limit load
p_{crack}	Constraint factor for reverse bending with respect to a crack
p_{notch}	Constraint factor for reverse bending with respect to a sharp notch
P_{RB}	Applied load in the reverse bending process
r	Distance from the notch tip, Radial coordinates at the notch tip
R	Stress ratio in fatigue precracking
$R\omega$	$(\omega_\varepsilon)^{L_r=1.35}/(\omega_\varepsilon)^{L_r=1.0}$
S	Bending span
S_L	Long span in four-point bending
S_S	Short span in four-point bending
T	CTOD test temperature
V_g	Clipgage displacement
W	Specimen width
YR	Yield ratio (yield stress/tensile stress)
α	Coefficient in Swift relationship
δ_{cr}	Critical CTOD value
$\delta_{cr,u}$	Scale parameter of critical CTOD value $\overline{\varepsilon_p}$, *PEEQ* Equivalent plastic strain
ε_z	Strain in the thickness direction
θ	Opening angle of the machined notch tip, Circumferential coordinates at the notch tip
ρ	Radius of the machined notch tip
σ_0	Reference stress in the Swift equation ($=\sigma_{YS}$)
σ_{comp}	Remote stress in the compression direction when reverse bending
σ_{flow}	Flow stress
$\sigma_{TS,T}$	Tensile strength at T (°C)
$\sigma_{TS,RT}$	Tensile strength at 293 °C
σ_{unload}	Stress at the notch tip during unloading after reverse bending
σ_{YS}	Yield stress
$\sigma_{YS,T}$	Yield stress at T (°C)
$\sigma_{YS,RT}$	Yield stress at 293 °C
σ_{yy}^{Hill}	Opening stress at the notch tip analyzed by Hill $\Delta\sigma_{eff}\sigma_{unload} - \sigma_{comp}$
$\overline{\sigma}$	Equivalent stress
φ	Tip angle of the envelope specified in the CTOD test standard
ω_{RB}	Plastically deformed area length at the root of the notch
ω_ε	Plastically deformed area length for a certain equivalent strain
ω^-	Plastically deformed area length under compressive stress in the Dugdale model
ω^+	Plastically deformed area length in the tensile direction during unloading after reverse bending

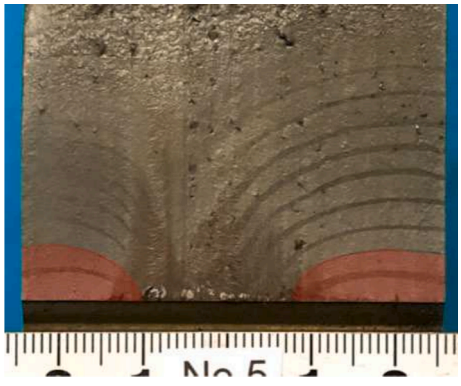

Fig. 1. An example of poorly fatigued precrack shapes for as-welded CTOD specimens with double-V edge preparation.

toughness testing of specimens was initiated in Japan in the last half of the 1970 s [6–8]. In the UK, the originator of the CTOD concept, as well as a leader in ISO CTOD test standard research, the reverse bending method is also referred to as “Japanese Reverse Bending” [9]. The reverse bending method has a substantial advantage in that it is quite easy to perform because the specimen is placed upside down in the same test machine as the CTOD test, and no large load is needed. The qualitative mechanism of fatigue crack shape improvement by reverse bending has been described previously, and many records indicate that the fatigue crack front shapes are straightened [2 10–13].

This technique was described in BS7448 part 2 [14], which was published in 1997; however, when this standard was transformed into ISO15653 in 2010, the description was deleted; this was the consequence of the decision of the ISO15653 project leader, who considered a report from Japan [15] (a typical figure is shown in Fig. 3), in which the difficulty of maintaining the crack front straightness requirement via reverse bending was revealed.

However, the demand for reverse bending is deeply rooted in the Japanese welding industry because of its simplicity. The Japanese Welding Engineering Society, where CTOD calculation formulas have

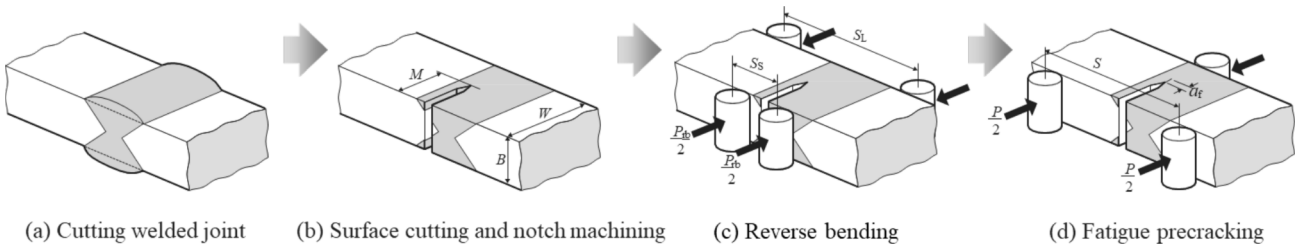

Fig. 2. Reverse bending process specified in ISO15653 for straightening the precrack shape of a weld CTOD specimen with residual stress distribution.

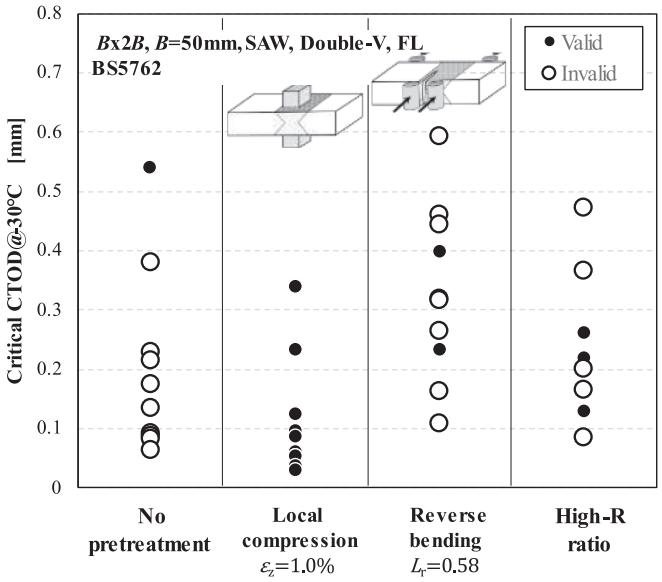

Fig. 3. CTOD test results for various crack front straightening techniques.

been developed [16–24], began to investigate whether reverse bending can be applied in multipass weld CTOD evaluations, as the detailed mechanism and the appropriate condition range were not known in 2016.

There are many studies on fatigue crack propagation, but we also referred to research on fatigue crack propagation behavior in residual stress fields [25] and on fatigue crack propagation criteria [26].

This series of papers summarizes the results of the research conducted by the Japanese committee. The principal author of these papers led the investigation of the reverse bending method; the objective was to establish the appropriate or recommended conditions for the utilization of this method.

This paper describes how fracture toughness changes with reverse bending when a 490 MPa steel base metal is used. In parallel, a three-dimensional finite element (FE) method is used to simulate the fracture toughness tests as closely as possible. The mechanism of the change in strain distribution and stress state in actual reverse bent specimens is discussed in detail. Finally, an appropriate upper limit of the reverse bend amount from the viewpoint of the fatigue crack shape is proposed.

2. Parameters describing the reverse bending conditions

2.1. Parameters

Reverse bending is the process of bending a CTOD specimen in the reverse direction to that of a CTOD test, i.e., closing the notch between notch machining and fatigue precrack introduction, as previously shown in Fig. 2. Through this process, tensile stresses can be distributed at the notch edge as a result of the unloading process after reverse bending. Consequently, fatigue cracks can be produced even at the center of the thickness where the residual stresses in the as-welded condition are distributed in the compressive direction. This phenomenon is a mechanical process that always occurs in materials with elasto-plastic properties, such as metallic materials.

The objective of this study is to specify an appropriate range of conditions for the use of reverse bending to ensure that the fracture toughness of welded joints with residual stresses is always adequately evaluated. The reverse bending condition is often described by using a limit load concept [27], which refers to the limit load at which the entire ligament yields under the assumption of an elastic-perfectly plastic beam with a notch. Although the authors recognize that this limit load deviates from the actual state due to strain hardening or constraint by a sharp notch or crack, the authors believe that this simple limit definition has the advantage of having a certain generality because it is a normalized expression for the thickness and length of the ligament. The present study follows this idea and uses the load ratio L_r shown in Eq. (1) to describe the amount of reverse bending. If the material behaves in an elastic-perfectly plastic property, L_r should not be greater than 1. However, the authors allow L_r to increase above 1 to reflect strain hardening of plasticity. That is, L_r is introduced as an indicator of the amount of bending.

$$P_{RB} = L_r P_L = L_r \cdot \frac{B\sigma_{YS,RT}(W - a_M)^2}{S - S_s} \tag{1}$$

(P_{RB}: reverse bending load, L_r: reverse bending load ratio, P_L: limit load, B: thickness, $\sigma_{YS,RT}$: yield stress at ambient temperature, W: specimen width, a_M: notch depth, S: outer span, and S_s: inner span)

Next, the fatigue precrack length is described in a form normalized by the ratio of the precrack length to the plastic deformation dimension (length on the crack line), k, as shown in Eq. (2), and is based on the region where the reverse bending plastic deformation counteracts the distribution of the welding residual stress. This concept is based on the work of Sakano [6–8], and it has been incorporated in Japanese studies [11 28 29] since the 1980 s. This form was described in BS7448-part2 [14] and appears in the current ISO 15653–2018 [4].

$$k = \frac{a_f}{\omega_{RB}} \tag{2}$$

(ω_{RB}: plastic zone length by reverse bending and a_f: fatigue precrack length).

The plastic zone length is determined based on some equations developed by Sakano [8], who first systematically theorized the reverse bending method. In Sakano's work, the plastic zone length for a three-point bending notched material is calculated by using a simple two-dimensional elastic–perfectly plastic material based on the Dugdale model [30], which is explained in detail in Appendix 1. Eqs. (3) – (5) show the formulas for deriving the final plastic zone dimensions. Based on the results of separate experiments, the constant L is set at 2.3, and the plastic zone length ω_{RB} can be calculated from the reverse bending load P_{RB}. The author is aware that $g_1(a_M/W)$ is a correction factor for three-point bending and that it differs slightly from four-point bending. However, the difference is limited, so this factor, which is used in CTOD calculations, is also used here to avoid complexity.

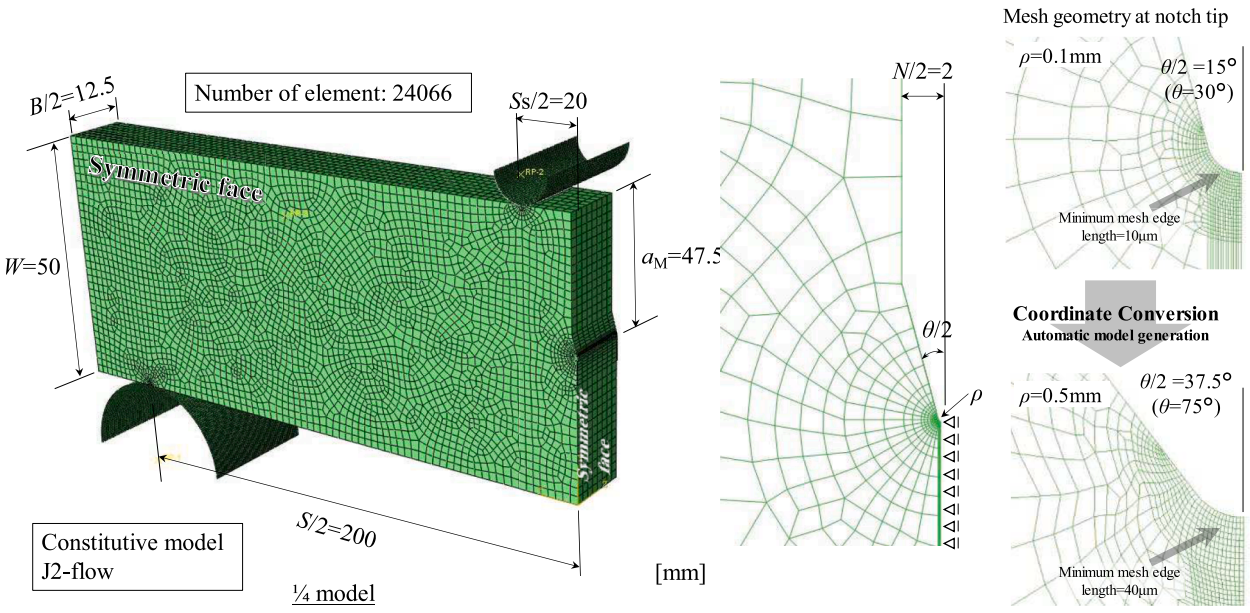

Fig. 4. FEM model for considering plastic zone dimensions in reverse bending.

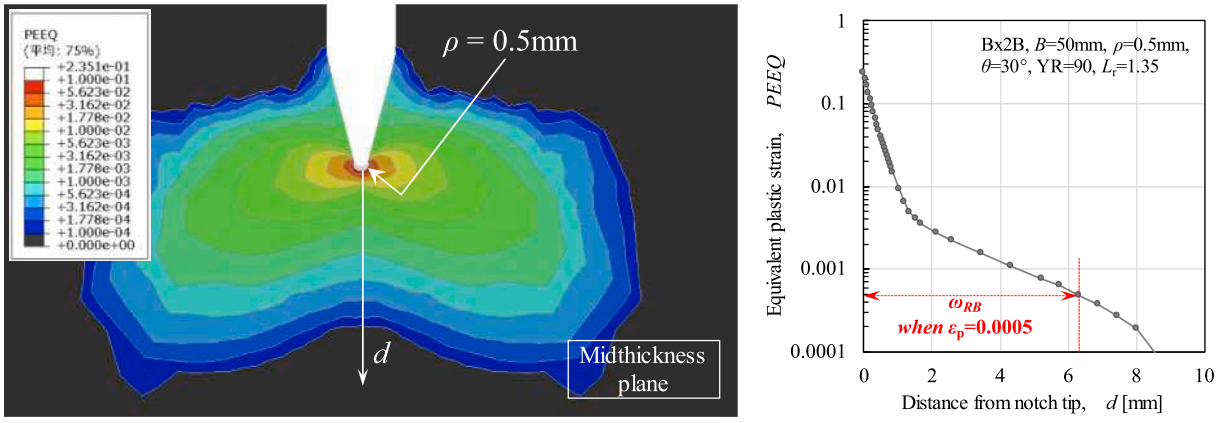

Fig. 5. Example of the equivalent plastic strain distribution at the notch tip during reverse bending.

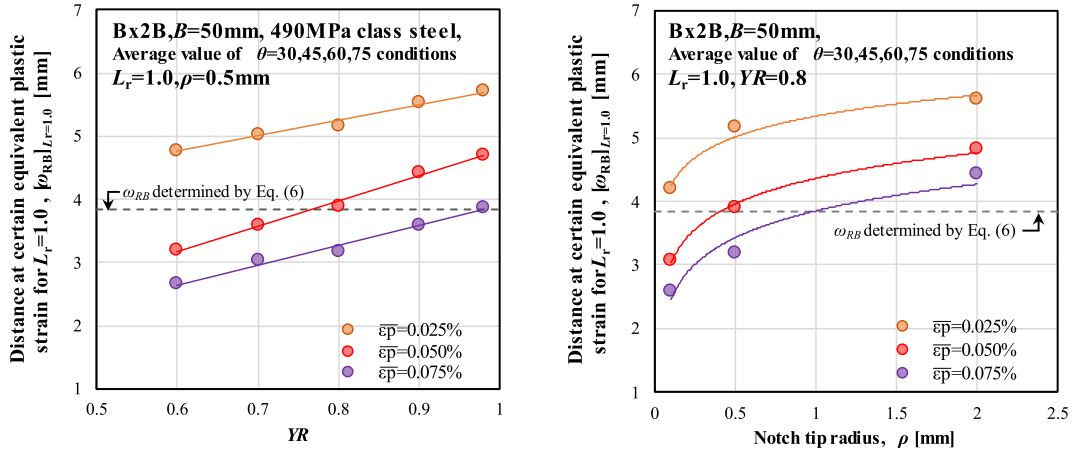

Fig. 6. Accuracy verification results of the plastic zone length via the simplified theoretical solution.

Table 1
Material profile used.

Thickness[mm]	Grade	Heat treatment[°C]	Chemical composition [mass%]					Tensile properties [MPa, –]		
			C	Si	Mn	P	S	$\sigma_{YS,RT}$	$\sigma_{TS,RT}$	*YR*
50	EH40	725 Water quench −600 Temper	0.12	0.32	1.29	0.006	0.003	359.5	473.5	0.759

$$\omega_{RB} = \frac{\pi}{8}\left(\frac{K_{RB}}{p_{notch}\cdot\sigma_{YS,RT}}\right)^2 \tag{3}$$

$$K_{RB} = \frac{P_{RB}(S-S_s)}{BW^{1.5}} g_1\left(\frac{a_M}{W}\right) \tag{4}$$

$$g_1\left(\frac{a_M}{W}\right) = \frac{3\left(\frac{a_M}{W}\right)^{0.5}\left[1.99 - \frac{a_M}{W}\left(1-\frac{a_M}{W}\right)\left\{2.15 - 3.93\frac{a_M}{W} + 2.7\left(\frac{a_M}{W}\right)^2\right\}\right]}{2\left(1+2\frac{a_M}{W}\right)\left(1-\frac{a_M}{W}\right)^{1.5}} \tag{5}$$

Accuracy check for simplified calculation of the plastic area length.

Equation (3) is a simplified elastic–plastic solution based on linear fracture mechanics and utilizes the Dugdale model; therefore, it may differ from the actual plastic zone dimensions. In this section, the accuracy of this estimation is evaluated via the finite element method (FEM). The model used for the analysis is shown in Fig. 4, where the notch angle and the notch tip curvature radius were varied. The stress–strain curves employed were based on six different types of virtual 490 MPa-class steels with varying work-hardening characteristics, as used by Kawabata et al [19]. FEM analysis is performed using Abaqus, which is based on the model in Fig. 5, by varying the notch angles and curvature changes. The equivalent plastic strain distribution in the plane at half the plate thickness in front of the notch is obtained, as shown in Fig. 6, and the plastic zone dimensions were calculated for each equivalent plastic strain threshold condition. The target for comparison in this analysis is the plastic zone dimensions proposed by Sakano et al. [8], as applied in this paper (Equation (3)). As is evident from Equation (6),

$$\sigma_{YS,T} = \sigma_{YS,RT}\exp\left[8\cdot10^{-4}\cdot(20+273)\left(\frac{\sigma_{YS,RT}}{E}\right)^{-1.5}\left\{\frac{1}{(T+273)\ln(10^8/10^{-4})} - \frac{1}{(20+273)\ln(10^8/10^{-4})}\right\}\right] \tag{7}$$

$$\sigma_{TS,T} = \sigma_{TS,RT}\exp\left[8\cdot10^{-4}\cdot(20+273)\left(\frac{\sigma_{TS,RT}}{E}\right)^{-1.5}\left\{\frac{1}{(T+273)\ln(10^9/10^{-4})} - \frac{1}{(20+273)\ln(10^9/10^{-4})}\right\}\right] \tag{8}$$

which is derived by substituting Equations (1) and (4), this equation provides a constant value that is determined based on the specimen width and notch length conditions and is independent of the notch geometry and material yield strength. The results obtained from the FEM are shown in Fig. 6 **(a)** and **(b)**. Upon comparing the results for multiple threshold conditions, the results approximately corresponded when the threshold condition is set at an equivalent plastic strain of 0.05 %. There is a slight variation depending on the crack tip geometry and material yield ratio (YR). In the theoretically derived plastic zone dimensions, the material's work-hardening characteristics and the constraint effect due to notch geometry, as outlined in Appendix 1, are simplified. As such, there may be some variability in accuracy depending on the case. However, the deviation is not significant, and the authors decided to use this simplified concept.

$$\omega_{RB} = \frac{\pi(W-a_M)^4}{8p_{notch}^2 W^3}\left\{g_1\left(\frac{a_M}{W}\right)\right\}^2 \tag{6}$$

3. Reverse bending experiments

Considering that the purpose of this study is to quantify the effect of reverse bending treatment on the fracture toughness evaluation, it is difficult to conduct tests using steel welded joints that actually require reverse bending. This is because the evaluation of welded joints is impossible without pretreatment, such as reverse bending. It is impossible to evaluate fracture toughness under each condition with and without reverse bending and compare both conditions. Therefore, in this work, the fracture toughness of welded joints with and without reverse bending is evaluated using a base metal specimen that can obtain valid fatigue precrack without pretreatment. Only the effects of reverse bending treatment and fatigue crack length are extracted and evaluated.

3.1. Materials

The steel plate used in the experiments is a 490 MPa-class structural steel with a thickness of 50 mm. Because of its high toughness, it is assumed that the evaluation temperature was extremely low, making evaluation difficult. Therefore, the steel is pretreated at 725 °C for 2 h, which is in the α-γ duplex phase, followed by water quenching and air cooling at 600 °C for 2 h. Table 1 shows the chemical composition and room temperature tensile properties of the specimens. To calculate the critical CTOD, the yield stress ($\sigma_{YS,T}$) and tensile strength ($\sigma_{TS,T}$) at the test temperature are needed, and the empirical temperature conversion equations [31], expressed by Eqs. (7) and (8), were used. Here, the ambient temperature is assumed to be 20 °C.

3.2. Results of the reverse bending and CTOD tests

For the reverse bending test, a standard CTOD specimen with a thickness of 50 mm is employed prior to introducing the fatigue crack. The specimen is placed in the testing machine via a four-point bending jig in the direction of the closing notch, as shown in Fig. 7. The specimens are subjected to two loading levels, where L_r is calculated to be 1.0 and 1.35 using the yield stress at room temperature shown in Table 2. The fatigue crack is allowed to propagate to various lengths under five different conditions. Here, a_f of R2 violates the minimum fatigue crack length requirement specified in ISO12135 [32], as shown in the Appendix. However, the authors confirm that the effect of this violation on the fracture driving force is limited, so no correction was made for the following discussion. A normal CTOD specimen without reverse bending is also prepared for meaningful comparison. The number of repetitions is set to 5 for all conditions. The test results for each condition are plotted on a Weibull probability paper in Fig. 8(a), and the results of arranging them as a cumulative distribution function assuming that the

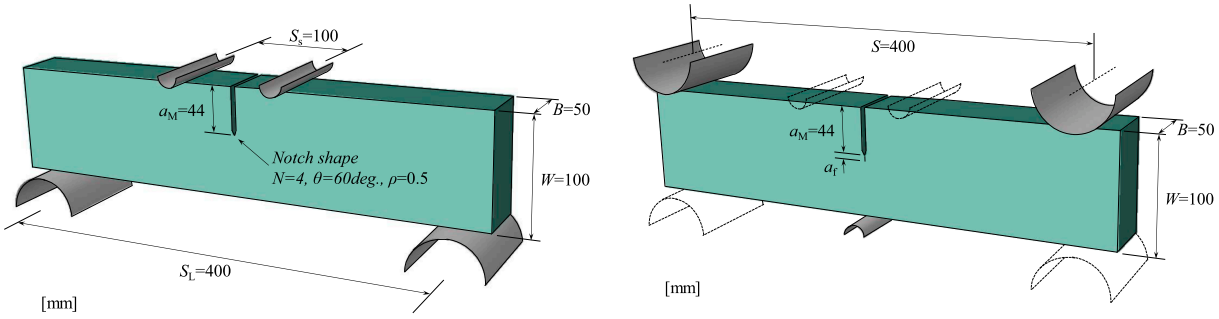

(a) 4-point reverse bend (b) CTOD test

Fig. 7. Configuration of the SEN(B) specimen and setup of the jigs.

Table 2
Reverse bend and fatigue precrack conditions.

Series	Number of specimens	Reverse bend	L_r	a_f [mm]	a_f/ω_{RB}
R1	5	N/A	–	4.53 ~ 4.85	–
R2	5	Yes	1.0	3.49 ~ 3.85	0.86 ~ 0.95
R3	5	Yes	1.0	7.51 ~ 7.77	1.85 ~ 1.92
R4	5	Yes	1.0	5.05 ~ 5.38	1.25 ~ 1.33
R5	5	Yes	1.35	6.34 ~ 6.56	0.87 ~ 0.92
R6	5	Yes	1.35	10.93 ~ 11.07	1.47 ~ 1.49

distribution follows the two-parameter Weibull distribution shown in Eq. (9) are shown in Fig. 8. The shape parameter m of the Weibull distribution is fixed at 2 based on the nature of cleavage fracture of steel materials [33,34], and the scale parameters $\delta_{cr,u}$ are determined using the least squares method. The resultant $\delta_{cr,u}$ and simple averaged value with each critical CTOD values are summarized in terms of L_r and a_f/ω_{RB} (=k) in Fig. 9. However, the arithmetic mean and the smallest critical CTOD values for L_r = 1.0 are less than those of the base material, whereas those for L_r = 1.35 seem to be much lower. For series R6, which shows the most significant decrease, the critical CTOD value decreases by more than 30 % on average.

$$F = 1 - \exp\left\{ -\left(\frac{\delta_{cr}}{\delta_{cr,u}}\right)^m \right\} \tag{9}$$

Photographs of the fracture appearance after the CTOD test are shown in Fig. 10. The observation of the fracture appearance of the specimens reveals that R5 and R6 at L_r = 1.35 have a slight concave curvature with a shortening of the crack shape at the center of the thickness of the base metal. The crack length difference, Δa_f, between the maximum fatigue precrack length, $a_{f,max}$, and the minimum length, $a_{f,min}\{i$ = 2–8$\}$, near the center of the thickness, is summarized in Fig. 11 for all specimens (Δa_f is set to zero when there is no concave shape). In Fig. 11, the horizontal axis is the fatigue crack length in the middle of the thickness (or the shortest length if the crack is concave), and the vertical axis is the amount of concavity (Δa_f). For L_r = 1.0, the crack does not become concave even at long lengths, whereas for L_r = 1.35, the crack growth seems delayed at the center of the thickness when it exceeds approximately 6 mm (approximately 0.8ω_{RB}). Considering that the specimen is a base metal with no residual stress, the fatigue crack delay at mid-thickness in the longer fatigue crack case suggests that L_r = 1.35 is an excessive reverse bending amount. This mechanism is explained via the numerical results in the next section.

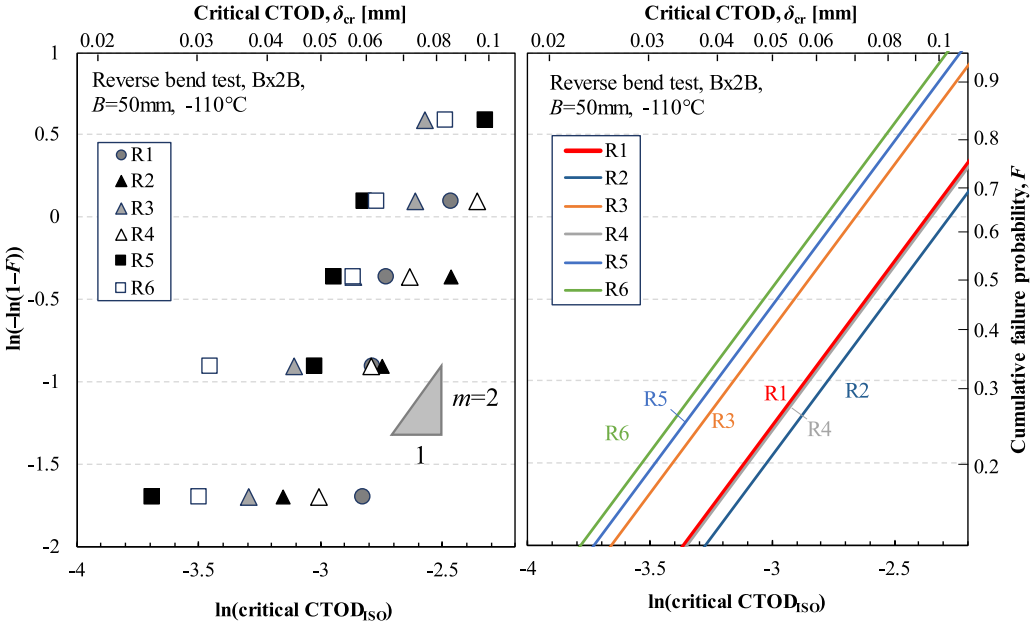

Fig. 8. Weibul distribution analysis for the CTOD test results for the RB specimens.

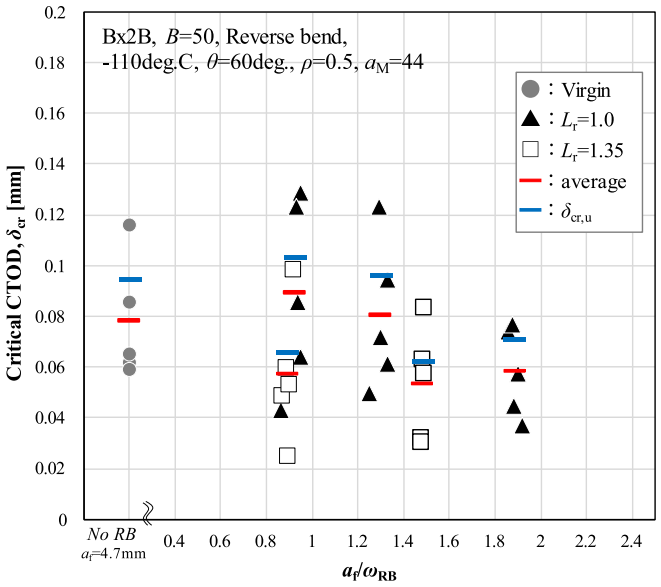

Fig. 9. CTOD test results for the RB specimens compared with the non-RB specimens.

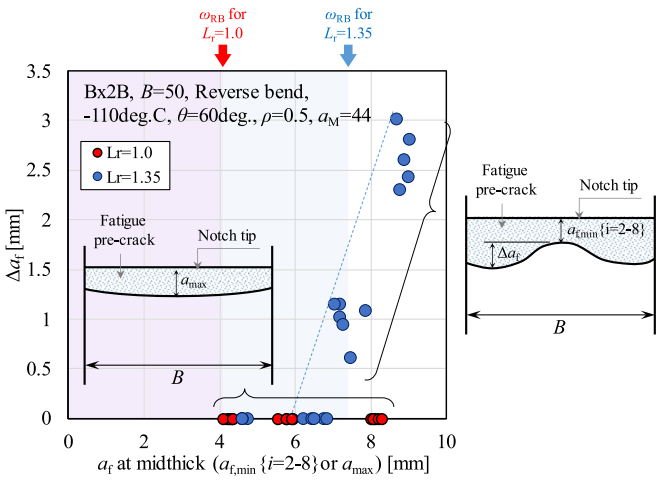

Fig. 11. Effects of the fatigue crack length and L_r condition on the straightness of the crack front.

4. Numerical simulation of experiments and discussion

4.1. Finite element analysis

A numerical analysis using the FE method is carried out to simulate the experiments described in the previous chapter. The stress–strain relationship used in the calculations is a Swift-type fitting of the results of tensile tests conducted at room temperature, as shown in Eq. (10). The stress–strain curve at the test temperature (T = –110 °C) is determined from the temperature equivalent of $\sigma_{YS,T}$ and $\sigma_{TS,T}$ via Eqs. (7) and (8) and the empirical correlation between the YR of the material and the Swift equations α and n for 490 MPa steel [19]. The stress–strain relationships at ambient and low temperatures used for FE analysis are shown in Fig. 12. Since the reverse bending process includes tensile and compressive cyclic loading, it is necessary to account for the Bauschinger effect (kinematic property) of the material. Fig. 13 shows an overview of the FE model used in the calculations. The model is constructed as closely as possible to the experiment; the mesh division scheme enables the opening profile behind the crack tip to be consistent with reality [19]. The elements are 8-node hexahedral isoparametric first-order elements, and Abaqus 2018 is used as the solver. The calculation steps are divided into four steps, as shown in Table 3. However, the nonstraight curvature of the fatigue crack shape is not considered, and it is assumed that the crack retains a two-dimensional shape of length a_0 at all thickness positions.

$$\bar{\sigma} = \sigma_0\left(1 + \frac{\bar{\varepsilon_p}}{\alpha}\right)^n \tag{10}$$

4.2. Changes in the stress–strain distributions of the specimens under reverse bending

Fig. 14 **(a)** and **(b)** show the stresses in the opening direction for L_r = 1.0 and L_r = 1.35, respectively, when the specimen is subjected to bending deformation in the notch closure direction. Fig. 15 shows the distribution of the equivalent plastic strain. The mechanism of the formation of the stress–strain state during each process is described below.

Series	R1	R2	R3	R4	R5	R6
RB condition	No RB	L_r=1.0			L_r=1.35	
Fatigue precrack length, $a_{f,av.}$	4.74	3.80	7.69	5.25	6.56	11.07
An example of fracture appearance	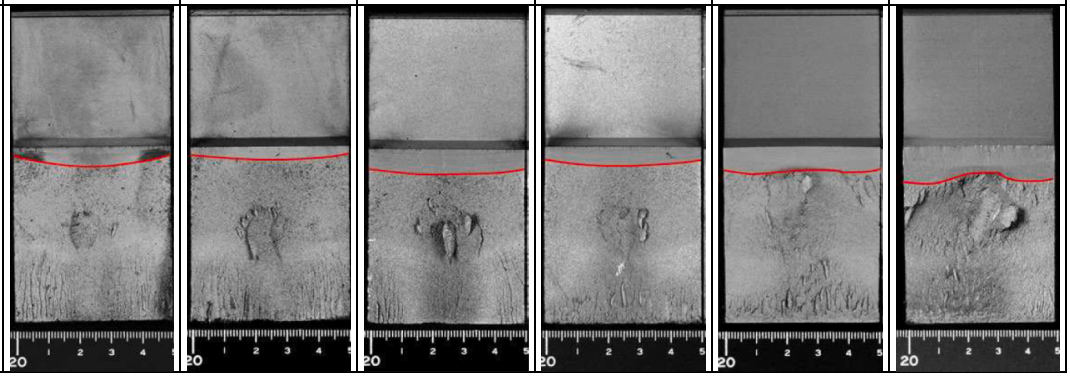					

Fig. 10. Fracture appearances of the specimens that exhibit the median critical CTOD value.

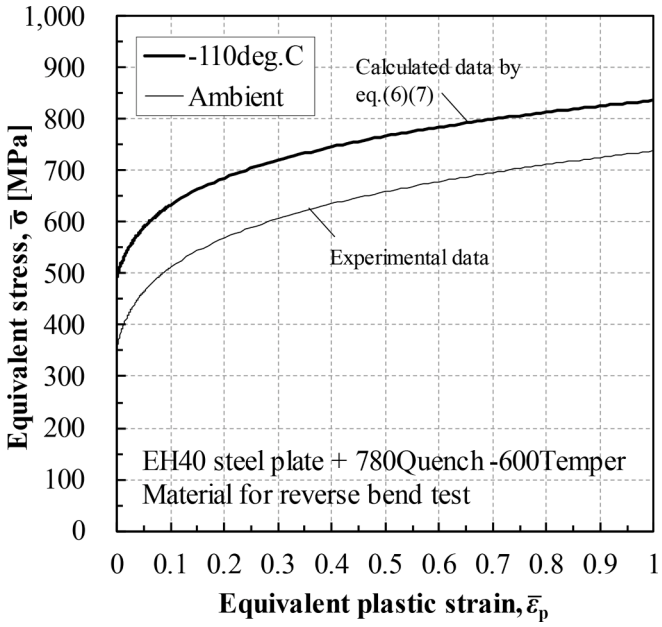

Fig. 12. Stress–strain relationships of the materials used.

4.2.1. Reverse bending

The compressive stress increases at the notch end because of reverse bending. Plastic deformation occurs from the notch end and the ligament end on the opposite side of the specimen. Considering the load index, L_r originally assumes an elastic–perfectly plastic material, and a plastic hinge condition is formed when $L_r = 1.0$. However, in practical steel with work hardening, there are still many regions where the interior is almost elastic at $L_r = 1.0$.

4.2.2. Unloading

The specimen attempts to return to its original shape by unloading. Nevertheless, since plastic deformation has been introduced at the notch end and the ligament end on the other side of the specimen, tensile stress was applied past the zero-stress state to return close to the original displacement. A schematic figure for the unloaded conditions using an elastic–perfectly plastic material model is shown in Fig. 16. The problem of bending plus unloading can be simplified to the superposition of (a) and (b) below. (a) represents bending, that is, bending deformation with plastic deformation at some of the upper and lower ends of the beam. (b) represents unloading, that is, the elastic reverse moment. In (c), S-shaped residual stresses are distributed under zero external load. Additionally, the stress increase and strain distribution at the notch root tend to be more pronounced because of the sharp notch at the top.

Table 3
FE calculation steps.

Step	Temperature
Reverse bending	Ambient
Unloading	Ambient
Cracking	Ambient⇒-110 °C
CTOD test	−110 °C

4.2.3. Precracking

The precracking process in this FE analysis is modeled via a simple node release method. This is because the plastic deformation associated with fatigue precrack propagation is considered negligible owing to its sufficiently small fatigue loads. Fig. 14 also shows the crack opening stress distribution at an average precrack length of all the reverse bending specimens (R2 ~ R6). The contribution of both the tensile residual stress introduced at the near-notch-root area and the compressive residual stress at the far-notch-root area changes with precrack length. In particular, the shorter the precrack length is, the stronger the tensile stress singular field at the crack tip; the longer the precrack length is, the more compressive the singular field becomes. These increasing and decreasing behaviors become more pronounced with increasing L_r.

Requirements for the fatigue crack length from the viewpoint of crack front straightness.

In this section, the residual stress distribution in front of the notch is discussed in detail via FE analysis. Figs. 17-18 show the distributions of crack opening stresses and equivalent plastic strains near the notch root at reverse bending, unloading, and fatigue precracking (assuming a straight crack front shape), respectively. First, a tensile residual stress distribution region at the near-notch-tip area forms during unloading,

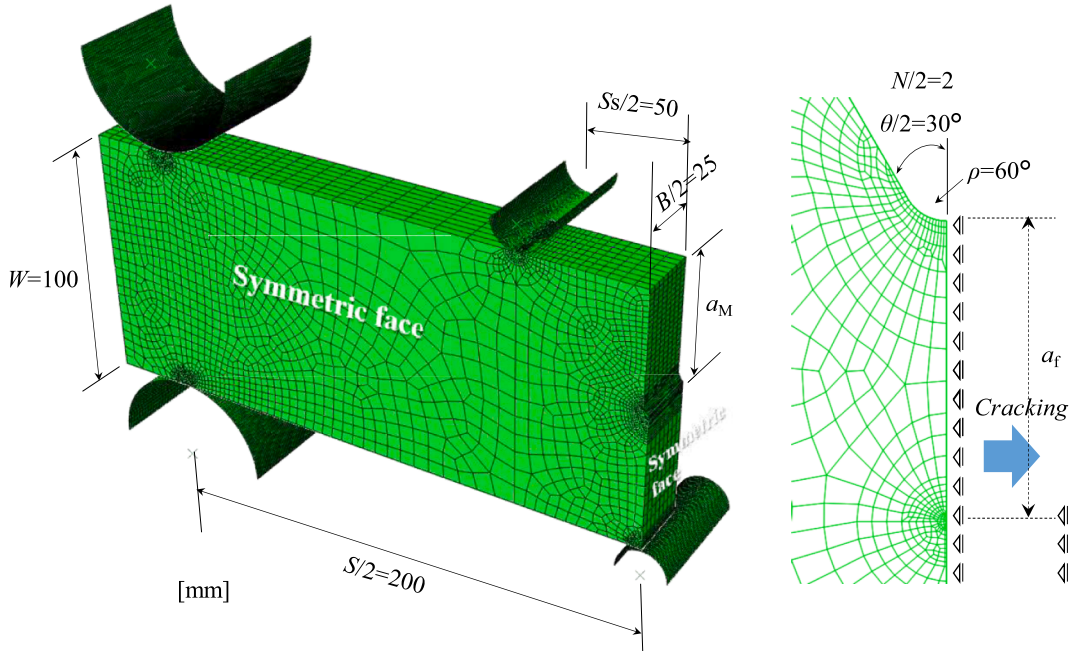

Fig. 13. FE model for the reverse bend and CTOD test simulations.

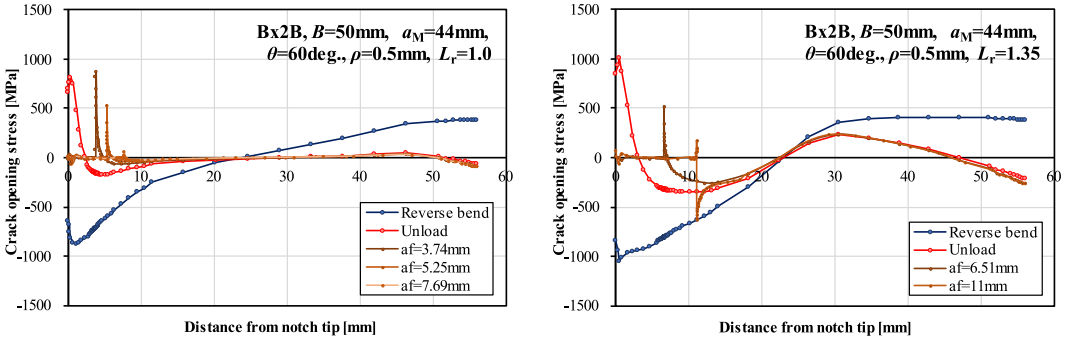

Fig. 14. Change in the opening stress distribution ahead of the notch tip.

which is crucial for promoting fatigue crack growth in the thickness position in the area of compressive residual stress, as shown in position (a) in Fig. 17. Focusing on the distribution of the equivalent plastic strain shown in Fig. 18, the region of plastic deformation grows larger in the $L_r = 1.35$ condition than in the $L_r = 1.0$ condition. For further discussion, the length of the area showing plasticity above a specific equivalent plastic strain is extracted from the distribution of the equivalent plastic strain in both conditions as a variable, ω_ε, and the ratio $R\omega$ of the lengths of the regions of equal plastic strain between the two L_r conditions is calculated via Eq. (11).

$$R_\omega = \frac{(\omega_\varepsilon)^{L_r=1.35}}{(\omega_\varepsilon)^{L_r=1.0}} \tag{11}$$

According to Sakano's assumption (Eq. (3)), the ratio is equal to the square of the amount of the load. However, this ratio is varied by the equivalent plastic strain level that is focused on due to the violation of the too simple assumption of Sakano's model, as shown in Fig. 19; this means that the length ratio is not proportional to the ratio of the plastic deformation area. To investigate the cause, Fig. 20 shows the distributions of compressive stress and strain in the thickness direction in the area of the notch bottom ligament during reverse bending. When L_r reaches 1.35, the tendency of the compressive stress distribution during reverse bending to become nonflat in the thickness direction becomes more pronounced; this is believed to be due to out-of-plane deformation, where the thickness increases on the front and back surfaces near the notch edge, the compressive stress in the thickness direction decreases, and the opening and closing stresses do not increase in the front and back surface regions. Therefore, when L_r is increased to 1.35, the compressive stress in the middle of the plate increases significantly, and the area where the fatigue crack propagates smoothly (a_f condition) does not expand proportionally according to Eq. (1). It is difficult to determine whether a toughness evaluation with a concave crack tip shape at the center of the thickness leads to conservative or unsafe results. Nevertheless, such conditions should be avoided in the evaluation.

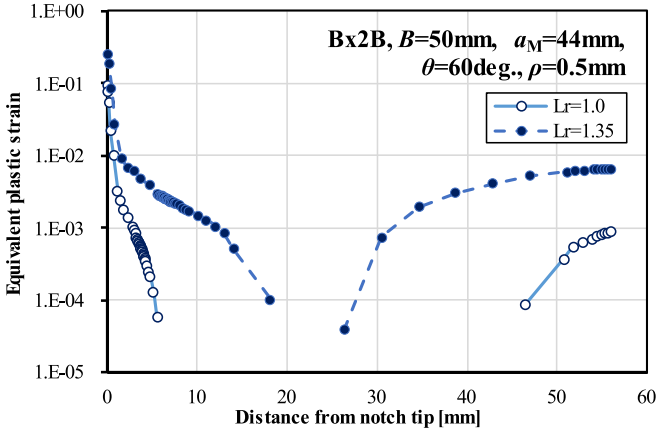

Fig. 15. Equivalent plastic strain distribution ahead of the notch tip.

4.3. Change in the load–clip gauge displacement (P–V_g) curve

As shown in Fig. 14, after reverse bending, nonnegligible residual stresses are distributed throughout the whole specimen. It is essential to investigate the variation in the P–V_g curve because the CTOD calculation in the ISO standard is based on the critical load and the geometric similarity of the specimen using the load–clip gauge displacement. Fig. 21 **(a)** shows the P–V_g curves obtained from the experiment. Fig. 21 **(b)** shows the P–V_g curves obtained from the FE analysis; the FE curves generally agree with the experimental data and support the correctness of the analysis. However, the slopes of the elastic lines greatly differ and

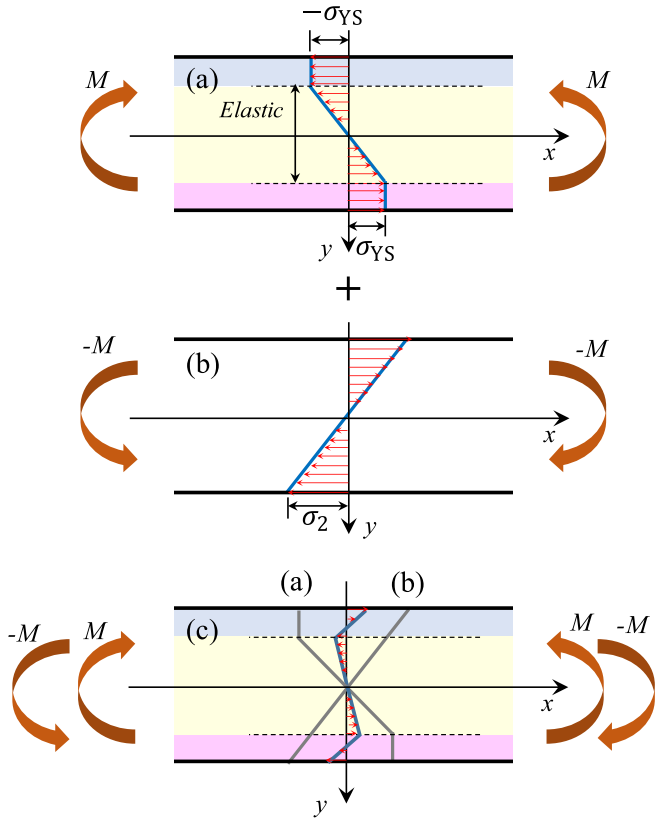

Fig. 16. Simplified explanation of bending and unloading in the elasto-plastic beam.

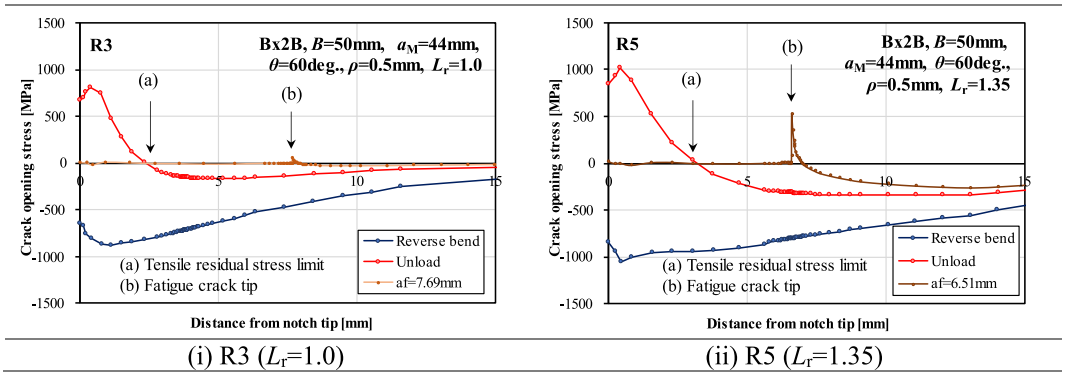

Fig. 17. Opening stress distribution ahead of the notch tip.

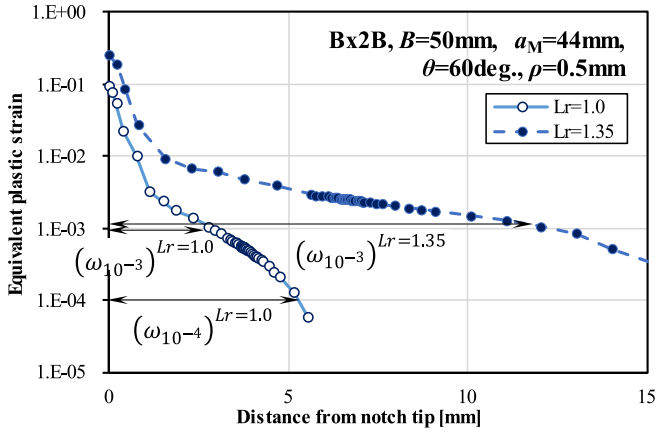

Fig. 18. Equivalent plastic strain distribution ahead of the notch tip for (L_r = 1.0 and 1.35) and definition of..$(\omega_\varepsilon)^{Lr}$

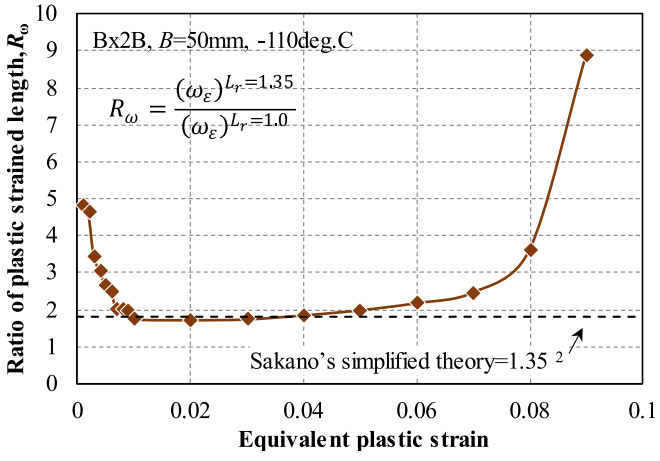

Fig. 19. Plastic strain region length ratio of the L_r = 1.35 condition for the L_r = 1.0 condition in reverse bend specimen.

are not suitable for discussing the effects of reverse bending alone. This is because the specimens have different crack depth ratios, a_0/W, because the fatigue precrack length is varied while the mechanical notch length is kept constant.

Therefore, additional FE analyses are carried out to investigate the change in the P–V_g curve under a fixed condition of a_0/W=0.5 and various reverse bending load and precrack length conditions. The results are shown in Fig. 22. For L_r = 1.0, there is almost no change in the shape of the curve compared with that of the nonreverse-bent specimen, but for L_r = 1.35, the curve tends to decrease, especially when the fatigue precrack is short (small k condition). The decrease in the load is pronounced around V_g = 1 but then returns to its original path. It can be inferred that the decrease is not due to kinematic hardening behavior (Bauschinger effect) but rather to the release of compressive residual stresses in the far-notch-root area, which is greater under high L_r conditions, as shown in Figs. 14 and 17. In the experimental results revealed in the previous section, the critical CTOD tends to decrease under high L_r conditions, but this decrease in the P–V_g curve displays the opposite effect. In any case, the purpose of the reverse bending treatment is to equalize the residual stresses in the welded joint at the notch tip and the evaluation area. Therefore, high L_r conditions close to 1.35 should not be selected because such a reverse bending process causes a marked distribution of compressive residual stresses over a wide area.

5. Conclusion

In this study, CTOD tests were carried out to clarify the effects of the reverse bending process, which is employed for CTOD testing of welded joints, on the assessment of critical CTOD values, fatigue precrack shapes, and P–V_g curve shapes. In addition, a three-dimensional FE method was employed to simulate the experiments, and the stress–strain distributions inside the specimens during each process were investigated to elucidate the mechanism of the reverse bending process. The results obtained in this study are summarized as follows:

1) Five types of CTOD tests with reverse bending were carried out on a 490 MPa base metal with a thickness of 50 mm at low temperatures, where the fracture mode is consistently brittle. The results were compared with the critical values of the base metal. The average critical CTOD values after reverse bending at L_r = 1.0 did not differ significantly from those of the base metal but were slightly lower at L_r = 1.35. However, discussing the effect of the reverse bend process is challenging, as these results encompass the influence of different conditions other than reverse bending (a_0/W, a_f).

2) The shape of the fatigue precrack front edges, as observed on the fracture surface of the specimens, indicates that at L_r = 1.0, the crack profile does not become concave even with prolonged extension. Nevertheless, at L_r = 1.35, crack growth is delayed at the center of the thickness when the crack extends to approximately 6 mm (approximately 0.8 ω_{RB}). Considering that the specimen is a base metal with no residual stresses, it is necessary to impose an upper limit on the fatigue crack length under high L_r conditions.

3) To obtain a detailed understanding of the changes in the stress–strain field introduced into the specimen during the reverse bending process, an FE model that can simulate the experiment as closely as possible was developed. After reverse bending and unloading, an S-shaped residual stress field formed in the specimen in the order of tension–compression–tension–compression starting from the notched root;

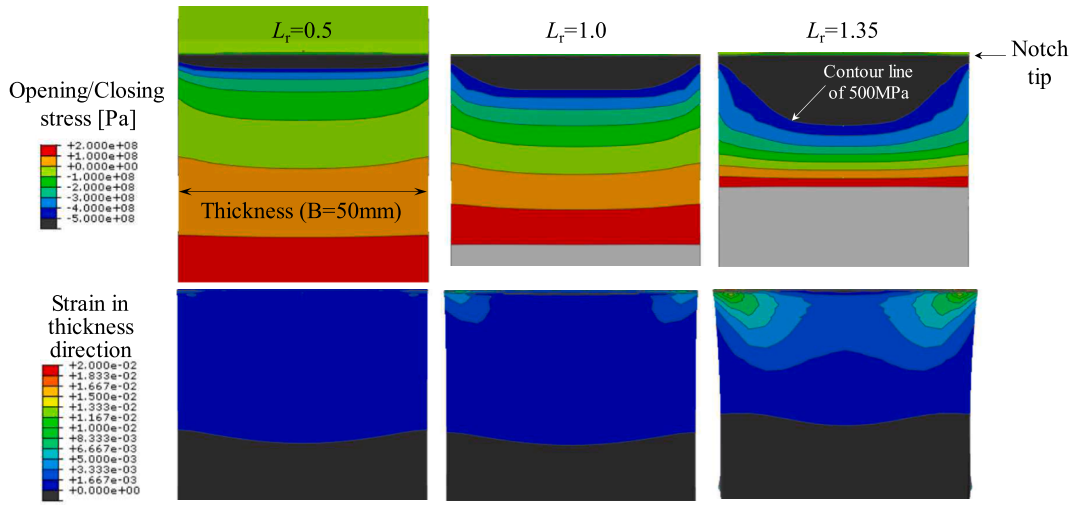

Fig. 20. Opening/closing stress and strain in the thickness direction in the ligament of the specimen after reverse bending (before unloading).

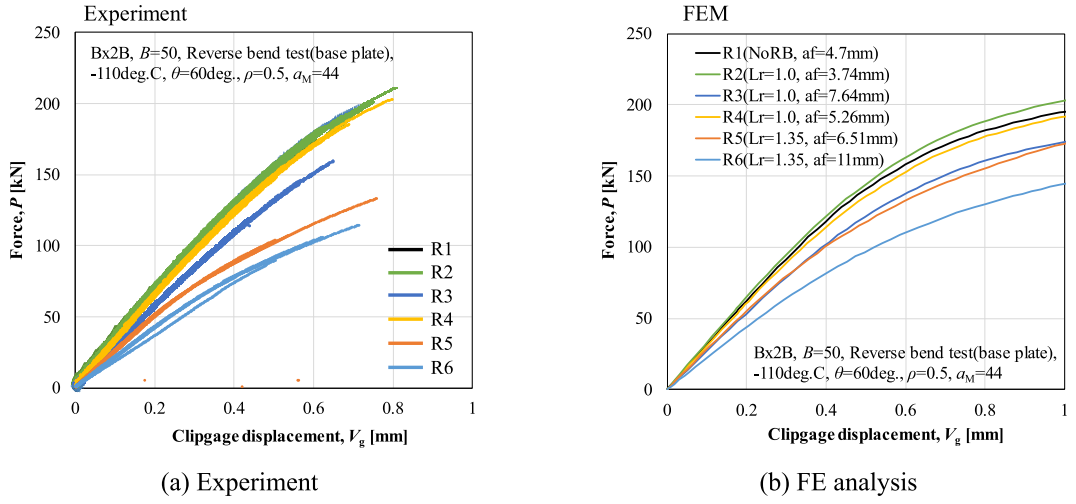

Fig. 21. Force–clipgage displacement curves from the experiments and FE simulations.

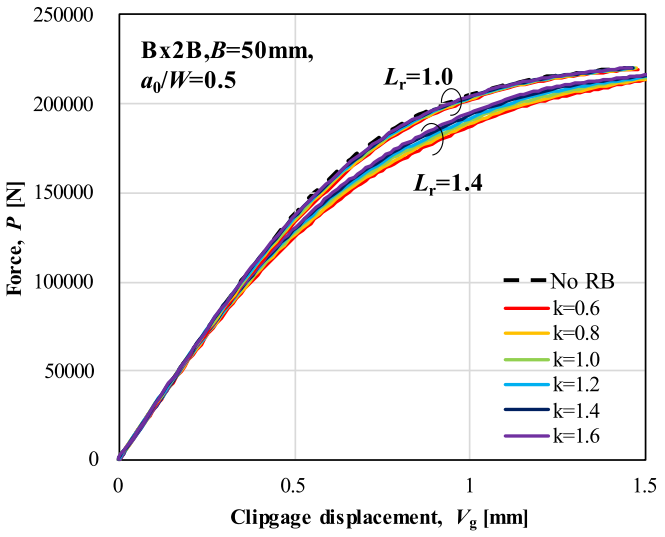

Fig. 22. Changes in the shape of the force–clipgage displacement curves under high-L_r conditions.

this is a common phenomenon in bending and unloading problems of elasto-plastic beams. In particular, the stress concentration effect at the notch root causes high tensile residual stress, which becomes the driving force for promoting crack growth at the thickness of the welded joint where compressive residual stress is distributed. The length of the tensile residual stress zone at the notch edge does not increase with increasing reverse bending load (L_r = 1.0 → 1.35). Instead, the compressive residual stresses distributed in front of the notch tend to increase and are not effective in flattening the precrack shape.

CRediT authorship contribution statement

Tomoya Kawabata: Writing – review & editing, Writing – original draft, Visualization, Validation, Supervision, Software, Resources, Project administration, Methodology, Funding acquisition, Formal analysis, Conceptualization. **Hoichi Kitano:** Validation, Methodology. **Takumi Ozawa:** Visualization, Validation, Software, Methodology. **Yoshiki Mikami:** Visualization, Validation, Supervision, Software, Methodology.

Declaration of competing interest

The authors declare that they have no known competing financial

interests or personal relationships that could have appeared to influence the work reported in this paper.

Acknowledgments

The authors wish to thank all members of the CTE committee of the Japan Welding Engineering Society for detailed and thorough discussions. This work was also supported by JSPS KAKENHI Grant Numbers 18H05337, 19H00802 and 24H00356.

Appendix A1. Sakano's solution for estimating the length of plastically deformed regions and validation via FEM analysis

Sakano clarified the relationship between stress and plastic zone length during reverse loading via the Dugdale model and derived the stress increase effect due to the presence of a notch by combining brittle fracture tests at low temperatures with the plastic constraint coefficient obtained from Hill's slip-line field theory [36]. Since this content holds significant importance to the main body of this paper, an outline is provided in this appendix.

Now, as shown in Fig. A1.1, consider a crack of length a_0 with singularity represented by the stress intensity factor K_{I0} in an ideal elastic–perfectly plastic body under uniform compression. Although only the positive region of the x-axis, which is the crack propagation direction, is depicted, a model with a symmetrical through-thickness defect in the negative x-region is also envisioned. Similar to Dugdale's method, assuming that point P is the virtual crack tip, the region of length ω^- behind the virtual crack tip can be substituted by a compressive force equivalent to the yield stress. At point P, since stress singularity does not occur, the sum of the stress intensity factor due to the external force and that acting on the crack plane must be zero. The stress intensity factor from the external load σ_{comp} ($\sigma_{comp} > 0$) is expressed by Equation (A1-1).

$$K_{\text{Remote stress}} = -\sigma_{comp}\sqrt{\pi(a_0+\omega^-)} \tag{A1-1}$$

Additionally, the stress intensity factor acting at a point on the crack plane is expressed via the coordinates and variables shown in Fig. A1.1 [7]. By superimposing this stress intensity factor over the load range, Equation (A1-3) can be obtained.

$$K_{\text{Point stress, } x} = 2\sqrt{\frac{a_0+\omega^-}{\pi}}\ \frac{\sigma_{YS,RT}}{\sqrt{(a_0+\omega)^2-x^2}} \tag{A1-2}$$

$$K_{\sum \text{Point stress}} = \int_{a_0}^{a_0+\omega} 2\sqrt{\frac{a_0+\omega^-}{\pi}}\ \frac{\sigma_{YS,RT}}{\sqrt{(a_0+\omega^-)^2-x^2}}dx \tag{A1-3}$$

Thus, the sum of Equations (A1-1) and (A1-3) must be zero. By simplifying this equation via substitution integration, Equation (A1-4) can be obtained.

$$\cos\left(\frac{\sigma_{comp}\pi}{2\sigma_{YS,RT}}\right) = \left(\frac{a_0}{a_0+\omega^-}\right) \tag{A1-4}$$

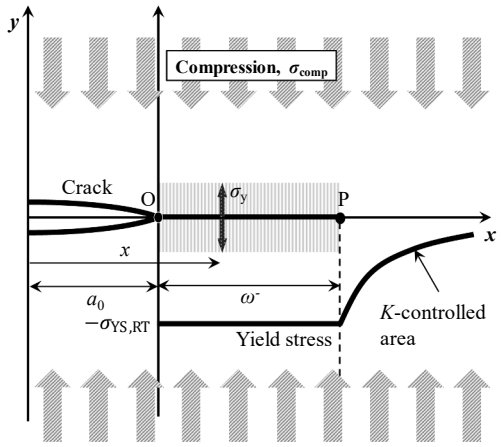

Fig. A1.1. Schematic stress distribution during reverse bending based on simplified Dugdale model

Considering the actual conditions of reverse bending, the defect of length a_0 is a sharp notch rather than a crack, thus requiring the integration of the stress distribution at the notch tip. Furthermore, as actual steel is not an elastic–perfectly plastic material but rather a work-hardening material, the integrated stress needs to be corrected from the yield stress to the effective stress. Hill's slip-line field analysis solution [36] for the sharp notch tip is given by Equations (A1-5) and (A1-6) is shown in Fig. A1.2.

$$\sigma_{yy}{}^{\text{Hill}} = \sigma_{YS}\left\{1+ln\left(1+\frac{r}{\rho}\right)\right\}\cdots\left(when\ \frac{r}{\rho}\le\exp\left(\frac{\pi}{2}-\theta\right)-1\right) \tag{A1-5}$$

$$\sigma_{yy}{}^{\text{Hill}} = \sigma_{YS}\left(1+\frac{\pi}{2}-\theta\right)\cdots\left(when\ \frac{r}{\rho}>\exp\left(\frac{\pi}{2}-\theta\right)-1\right) \tag{A1-6}$$

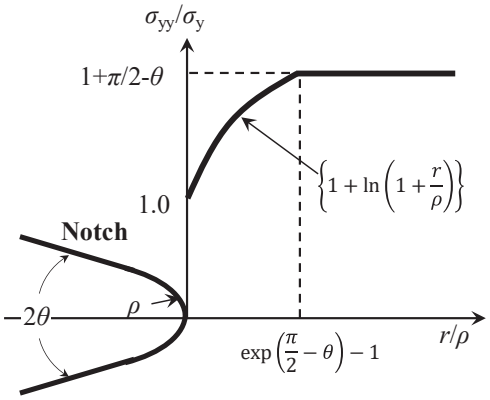

Fig. A1.2. Stress distribution in the opening direction based on slip line field analysis [36].

The yield stress, assumed to be constant in Equation (A1-4), can be rewritten using Equation (A1-6) with the average flow stress σ_{flow}, derived from ${\sigma_{yy}}^{\text{Hill}}$ over the integration range, as shown in Equation (A1-5).

$$\cos\left(\frac{\sigma_{\text{comp}}\pi}{2\sigma_{\text{flow}}}\right)=\left(\frac{a_0}{a_0+\omega^-}\right) \tag{A1-5}$$

$$\sigma_{\text{flow}}\approx\frac{1}{\omega^-}\int_{a_0}^{a_0+\omega^-}{\sigma_{yy}}^{\text{Hill}}dx \tag{A1-6}$$

Therefore, the desired plastic zone length ω^- can be calculated considering the notch shape (θ, ρ) using Equation (A1-5).

Next, Hill's simplified stress distribution model at the notch tip, as examined experimentally by Sakano, is introduced. After reverse bending and unloading, the tensile stress distribution partially remains at the notch tip. However, as compressive stress is broadly distributed ahead, cracks, if initiated at the notch tip, eventually stop. Sakano conducted experiments to select temperatures and materials where brittle crack propagation-stopping occurs upon simple unloading after reverse bending, revealing the strain-hardening status at the notch bottom experimentally. This situation is schematically shown in Fig. A1.3. Here, the external force is denoted as the unloading stress σ_{unload}, and considering that there is no stress singularity at the tip position R of the tensile plastic deformation zone generated from crack tip Q after stopping, a simplified mathematical approach based on the Dugdale model similar to reverse bending yields Equation (A1-7). Here, $K_{\Delta\sigma}$ represents the K value change due to effective stress variation $\Delta\sigma_{\text{eff}}\left(\sigma_{\text{unload}}-\sigma_{\text{comp}}\right)$, and K_R represents the K value due to residual stress acting around the initial crack tip in the baseline state between points OR, whereas $K_{\sum\text{Point stress}}$ represents the K value due to the closing force acting over the QR range.

$$K_{\Delta\sigma_{\text{eff}}}+K_R+K_{\sum\text{Point stress}}=0 \tag{A1-7}$$

As in the case of compressive loading, the K value is calculated via the splitting force equation [35] to derive the following expression.

$$\Delta\sigma_{eff}\sqrt{\pi(a_0+\Delta a+\omega^+)}+\int_{a_0}^{a_0+\Delta a+\omega^+}\frac{-p_{\text{notch}}\sigma_{\text{YS,T}}}{\sqrt{(a_0+\Delta a+\omega^+)^2-x^2}}dx+\int_{a_0+\Delta a}^{a_0+\Delta a+\omega^+}\frac{-p_{\text{crack}}\sigma_{\text{YS,T}}}{\sqrt{(a_0+\Delta a+\omega^+)^2-x^2}}dx=0 \tag{A1-8}$$

Here, p_{notch} and p_{crack} are coefficients representing the ratio of σ_{flow} to $\sigma_{\text{YS,T}}$ on the basis of Hill's analysis. Sakano refers to these coefficients as plastic constraint coefficients. This integral yields

$$\frac{\pi\Delta\sigma_{eff}}{2\sigma_{\text{YS,T}}}=p_{\text{notch}}cos^{-1}\left(\frac{a_0}{a_0+\Delta a+\omega^+}\right)+p_{\text{crack}}cos^{-1}\left(\frac{a_0+\Delta a}{a_0+\Delta a+\omega^+}\right) \tag{A1-9}$$

Assuming that the constant critical tensile plastic zone length ω_c^+ can be applied as the crack initiation criterion [37] and given that $\Delta a\ll a_0$, $\omega\cong\omega_c^+$. By experimentally collecting numerous records of crack propagation-stopping during unloading after reverse bending, p_{notch} can be obtained. In tests in which reverse bending was used on actual 490 MPa- and 780 MPa-class steels, despite the use of specimens with varying notch angles, there was little difference in crack length based on the notch angle. The simplified theoretical solution could explain the phenomenon when the notch angle 2θ was 30°. Thus, substituting $\theta=15^\circ$ into Equation (A1-6) yields $p_{\text{notch}}=2.3$, which was taken as the average strain hardening rate for general notch bottoms.

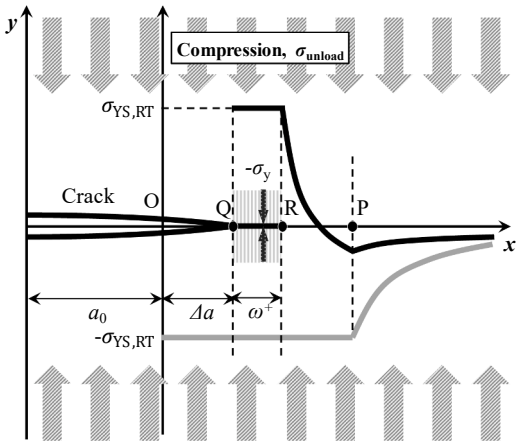

Fig. A1.3. Schematic stress distribution during unloading of brittle crack initiation and stopping, which is based on simplified Dugdale model

This paper emphasizes determining the plastic zone at the notch tip. The simplest method, Equation (A1-10), which is based on linear fracture mechanics (small-scale yielding conditions), was used, adopting the value obtained by multiplying the yield stress by the plastic constraint coefficient p_{notch} (=2.3) as the effective flow stress (Equation (A1-12)). This method has been adopted as a plastic zone length calculation method for reverse bending in BS7448 Part 2–1994.

$$\omega = \frac{\pi}{8}\left(\frac{K}{\sigma_{flow}}\right)^2 \tag{A1-11}$$

$$\omega = \frac{\pi}{8}\left(\frac{K}{p_{notch}\sigma_{YS,RT}}\right)^2 = \frac{\pi}{8}\left(\frac{K}{2.3\sigma_{YS,RT}}\right)^2 \tag{A1-12}$$

Appendix A2. The envelope requirements specified in ISO12135

A CTOD test is carried out after a fatigue precrack is introduced into a mechanically notched specimen. The fracture driving force at the crack tip is reduced if the fatigue crack length is too short compared with the case where all the defect regions consist only of cracks without notches [38]; therefore, the fatigue crack should be long enough (the stress intensity factor in the SIF formula [39] and CTOD formula [32] does not account for the effect of the proximity of notches and crack tips). Fig. A2.1 illustrates the situation of fatigue precrack growth at the notch root and the envelope rule. The notch must fit inside the envelope shown by the dashed line. Here, the function *f* is the distance between points A and B (defined as a positive number if the notch is contained in the envelope). Eq. (A2-1) can be derived from the condition that the function *f* is a positive number. This equation is illustrated in Fig. A2.1, where *N* is a variable and the possible regions of a_f are shown under the condition that the tip radii of curvatures ρ and φ are fixed.

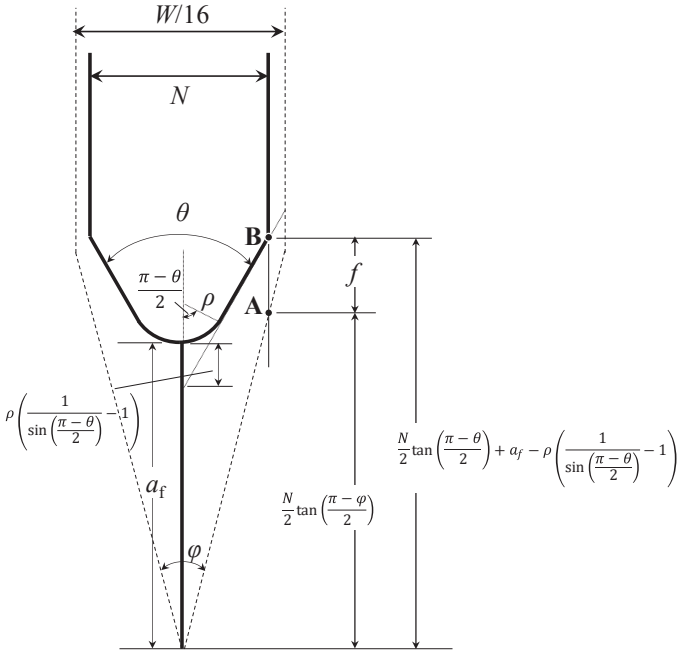

Fig. A2.1. Envelope requirements of the CTOD test standards and definition of function f

$$a_f \geq \frac{N}{2}\left\{\tan\left(\frac{\pi-\varphi}{2}\right)-\tan\left(\frac{\pi-\theta}{2}\right)\right\}+\rho\left\{\frac{1}{\sin\frac{\theta}{2}}-1\right\} \quad \text{(A2-1)}$$

Data availability

Data will be made available on request.

References

[1] A. Wells, Unstable crack propagation in metals: cleavage and fast fracture, in: Proceedings of the crack propagation symposium, Vol. 1, No. 84, Cranfield, UK, 1961, p. p. 26028)..

[2] O.L. Towers, M.G. Dawes, Welding Institute research on the fatigue precracking of fracture toughness specimens, Elastic-Plastic Fracture Test Methods: The User's Experience, ASTM STP 856 (1985) 23–46.

[3] CTE committee internal report, Japanese Welding Engineering Society, 2019 (internal report, in Japanese).

[4] International Organization for Standardization, "Method of test for the determination of quasistatic fracture toughness of welds," ISO15653 (2018).

[5] C.T. Fujii, E.A. Metzbower, Stress-Corrosion Cracking of Steel Weldments, Metals Engineering Quarterly 16 (4) (1976) 15–20.

[6] K. Sakano, Precompression cracking method for fracture toughness test, *Journal of the Society of Naval Architects of Japan* 141 (1977) 282–289. In Japanese.

[7] K. Sakano, A study on the crack initiation and propagation in a precompressed notched specimen, *Journal of the Society of Naval Architects of Japan* 1978 (143) (1978) 446–453. In Japanese.

[8] K. Sakano, Precompression Cracking Method for Fracture Toughness Test (2nd Report), Journal of the Society of Naval Architects of Japan 144 (1978) 352–361. In Japanese.

[9] H.S. Reemsnyder, H.G. Pisarski, M.G. Dawes, Residual stresses and fatigue precracking techniques for weldment fracture toughness specimens, *J. Test. Eval.* 20 (6) (1992) 416–423.

[10] S. Jeong, H.S. Kim, S.B. Shin, T.J. Park, Effect of reverse bending method on pre-crack straightness in CTOD test of welded thick steel plates, in: ASME International Mechanical Engineering Congress and Exposition, Vol. 46583, American Society of Mechanical Engineers, 2014 V009T12A029.

[11] FTR committee final report, Japanese Welding Engineering Society, 1985 (internal report, in Japanese).

[12] Y. Mikami, T. Kawabata, A. Kiuchi, T. Tagawa, H. Kitano, S. Kanna, S. Aihara, Y. Kayamori, Y. Imai, M. Mochizuki, M. Ohata, Y. Hagihara, T. Sakurai, F. Minami, Numerical simulation of residual stress modification by reverse bending of notched fracture toughness test specimens of multipass welds, *Theor. Appl. Fract. Mech.* 92 (2017) 214–222.

[13] T. Tagawa, Y. Morikage, T. Kubo, T. Handa, Y. Mikami, T. Kawabata, Experimental proof of reverse bending technique for modifying weld residual stress in weld CTOD specimen and comparison of effect with other techniques, Journal of Testing and Evaluation 49 (6) (2021) 4230–4247, https://doi.org/10.1520/JTE20200577.

[14] British Standard BS7448 – Part 2, "Fracture mechanics toughness tests – Part 2. Method for determination of K_{IC}, critical CTOD and critical J values of welds in metallic materials," (1997).

[15] S. Machida, T. Miyata, M. Toyosada, Y. Hagiwara, Study of methods for CTOD testing of weldments, in: Fatigue and fracture testing of weldments, ASTM International, 1990, pp. 142–156.

[16] T. Tagawa, Y. Kayamori, M. Ohata, Y. Yamashita, T. Handa, T. Kawabata, K. Tsutsumi, H. Yoshinari, S. Aihara, Y. Hagihara, Difference between ASTM E1290 and BS 7448 CTOD Estimation Procedures, *Weld. World* 54 (7–8) (July 2010) R182–R188, https://doi.org/10.1007/BF03263504.

[17] T. Tagawa, Y. Kayamori, M. Ohata, T. Handa, T. Kawabata, Y. Yamashita, K. Tsutsumi, H. Yoshinari, S. Aihara, Y. Hagihara, Comparison of CTOD standards: BS 7448-Part 1 and revised ASTM E1290, *Eng. Fract. Mech.* 77 (2) (2010) 327–336, https://doi.org/10.1016/j.engfracmech.2009.02.009.

[18] T. Tagawa, T. Kawabata, T. Sakimoto, Y. Kayamori, M. Ohata, Y. Yamashita, E. I. Tamura, H. Yoshinari, S. Aihara, F. Minami, H. Mimura, Experimental measurements of deformed crack tips in different yield-to-tensile ratio steels, Engineering Fracture Mechanics 128 (2014) 157–170, https://doi.org/10.1016/j.engfracmech.2014.07.012.

[19] T. Kawabata, T. Tagawa, T. Sakimoto, Y. Kayamori, M. Ohata, Y. Yamashita, E. Tamura, H. Yoshinari, S. Aihara, F. Minami, H. Mimura, Y. Hagihara, Proposal for a new CTOD calculation formula, *Eng. Fract. Mech.* 159 (July 2016) 16–34, https://doi.org/10.1016/j.engfracmech.2016.03.019.

[20] T. Kawabata, T. Tagawa, Y. Kayamori, M. Ohata, Y. Yamashita, M. Kinefuchi, H. Yoshinari, S. Aihara, F. Minami, H. Mimura, Y. Hagihara, Plastic deformation behavior in SEB specimens with various crack length to width ratios, *Eng. Fract. Mech.* 178 (1) (June 2017) 301–317, https://doi.org/10.1016/j.engfracmech.2017.03.029.

[21] T. Kawabata, T. Tagawa, Y. Kayamori, M. Ohata, Y. Yamashita, M. Kinefuchi, H. Yoshinari, S. Aihara, F. Minami, H. Mimura, Y. Hagihara, Applicability of new CTOD calculation formula to various a_0/W conditions and B×B configuration, *Eng. Fract. Mech.* 179 (15) (June 2017) 375–390, https://doi.org/10.1016/j.engfracmech.2017.03.027.

[22] T. Kawabata, T. Tagawa, Y. Kayamori, Y. Mikami, H. Kitano, A. Kiuchi, S. Kanna, T. Sakurai, Y. Imai, M. Ohata, M. Mochizuki, F. Minami, S. Aihara, Y. Hagihara, Investigation on η and m Factors for J Integral in SE(B) Specimens, *Theor. Appl. Fract. Mech.* 97 (October 2018) 224–235, https://doi.org/10.1016/j.tafmec.2018.08.013.

[23] T. Kawabata, Y. Kayamori, T. Tagawa, A proposal of the CTOD calculation formula and its conversion factor to J-integral in C(T) specimens, *Mater. Perform. Charact.* 9 (5) (October 2020) 608–626, https://doi.org/10.1520/MPC20190196.

[24] T. Kawabata, H. Kosuge, T. Ozawa, Y. Mikami, Simplified prediction method of Stress Intensity Factor in mid-thick plane in 3D cracked body and its difference from 2D handbook formula, *J. Test. Eval.* 08 (June 2021), https://doi.org/10.1520/JTE20210006.

[25] K. Werner, The fatigue crack growth rate and crack opening displacement in 18G2A-steel under tension, Int. J. Fatigue 392 (2012) 25–31, https://doi.org/10.1016/j.ijfatigue.2011.06.005.

[26] D. Rozumek, Influence of the slot inclination angle in FeP04 steel on fatigue crack growth under tension, Mater. Des. 30 (6) (2009) 1859–1865, https://doi.org/10.1016/j.matdes.2008.09.017.

[27] Dowling, N. E., Mechanical Behavior of Materials: Engineering Methods for Deformation, Fracture, and Fatigue, Prentice Hall College Div (1993/01), ISBN-10: 0135790468.

[28] Kawabata, T., Plastic strain distribution in reverse bent SEN(B) specimen and prediction accuracy by Sakano's simplified calculation formula, An internal report in CTE committee (in Japanese).

[29] FTW committee final report, Japanese Welding Engineering Society, 1990 (internal report, in Japanese).

[30] D.S. Dugdale, Yielding of steel sheets containing slits, *J. Mech. Phys. Solids* 8 (2) (1960) 100–104, https://doi.org/10.1016/0022-5096(60)90013-2.

[31] Japanese Welding Engineering Society, Method of assessing brittle fracture in steel weldments subjected to large cyclic and dynamic strain, *WES2808*, 2017.

[32] International Organization for Standardization (ISO), Unified method of test for the determination of quasistatic fracture toughness, ISO12135 (2016), (2021).

[33] K. Wallin, The scatter in KIC-results, Eng. Fract. Mech. 19 (6) (1984) 1085–1093, https://doi.org/10.1016/0013-7944(84)90153-X.

[34] T. Ozawa, T. Kawabata, Y. Mikami, Proposal of new MOTE methods for brittle fracture toughness determination, ISIJ Int. 62 (6) (2022) 1301–1311, https://doi.org/10.2355/isijinternational.ISIJINT-2021-579.

[35] G.R. Irwin, Analysis of stresses and strains near the end of a crack traversing a plate, *Journal of Applied Mechanics* 24 (1957) 361.

[36] R. Hill, The Mathematical Theory of Plasticity, Oxford University Press, Oxford, 1950.

[37] F. Koshiga, A proposed mechanism of brittle fracture initiation influenced by overstressing techniques in terms of Dugdale model, Journal of the Society of Naval Architects of Japan 1970 (127) (1970) a239–a245.

[38] T. Rich, R. Roberts, Plastic enclave sizes for internal cracks emanating from circular cavities within elastic plates, *Eng. Fract. Mech.* 1 (1) (1968) 167–173.

[39] J.E. Srawley, Wide range stress intensity factor expressions for ASTM E399 standard fracture toughness specimens, *Int. J. Fract.* 12 (3) (1976) 475.